

Supplementary information

Chemicals and handling

All chemicals were of reagent grade (Sigma Aldrich) and next purification was not necessary. The ligand bis(diphenylphosphan)methane was received in non-oxidized form (Figure S1). Anhydrous $CoBr_2$ was used in synthesis.



Figure S1. Structure of the free, non-oxidized ligand *dppm*.

Physical Measurements

C, H and N content in the complex was determined by microanalytical method (Thermo Electron Flash EA 1112). IR spectrum was recorded using FT-IR spectrometer (Nicolet 5700, Thermo Scientific) in the region $400 - 4000\text{ cm}^{-1}$ at room temperature in a dried KBr pellet. Electronic spectrum was collected in region $9000 - 50\,000\text{ cm}^{-1}$ of the powdered samples in Nujol oil (Specord 200, Analytical Jena).

Synthesis of $[Co(dppm^{O,O})_3][CoBr_4]$ (**1**)

A 100 cm^3 round-bottomed flask was charged with non oxidized form of ligand bis(diphenylphosphan)methane (0.150 g, 0.390 mmol) dissolved in acetonitrile (20 cm^3). After 10 min an anhydrous $CoBr_2$ (0.043 g, 0.195 mmol) was added once. The mixture was stirred and heated up at 80°C for 4 hours without protection of air. The colour changed slowly from light blue to its dark. The hot mixture was filtered and allowed to stand at room temperature for one week. Well shaped crystals were separated and dried between wood pulp in the oven at 40°C . Data for **1**. Yield: 0.11 g, 17 %, blue rhomboids. Melting point: $241 - 243^\circ\text{C}$. Selected FT-IR bands (1.32 mg / 250 mg KBr, rt): $\nu/\text{cm}^{-1} = 3462, 3055, 2925, 2868, 2241, 1589(\text{m}), 1483(\text{m}), 1438(\text{s}), 1356, 1334, 1313, 1158(\text{s}), 1123(\text{m}), 1098, 1070, 1028, 997(\text{m}), 790(\text{s}), 741(\text{s}), 691(\text{s}), 569(\text{m}), 504(\text{s})$ (s – strong, m – medium). UV/Vis (Nujol, rt) $\nu_{\text{max}}/10^3\text{ cm}^{-1}$ (relat. absorb.): 13.77(1.279), 14.22(1.252), 14.95(1.0954), 17.89(0.261). Elemental analysis calc. $C_{75}H_{66}Br_4Co_2O_6P_6$ (1686.59 g mol⁻¹): C, 53.4; H, 3.9. Found: C, 53.3; H, 4.1 %.

Structural data

Single crystal X-ray diffraction measurements and data collection for *dppm* and **1** were carried out using the Eulerian-cradle diffractometer Stoe StadiVari using Pilatus 300K HPAD detector and CuK α radiation microfocus source Xenocs Genix3D at 100 K. The diffraction intensities were corrected for Lorentz and polarization factors. The structure was solved by charge-flipping and direct methods with SUPERFLIP and SHELXT.^{S1,S2} and refined by the full-matrix least squares procedure with SHELXL (version 2016/6).^{S3} The crystal structure was drawn using the OLEX2 and MERCURY programs.^{S4,S5} Crystal data, conditions of data collection and refinement are reported in Table S1. All atoms in $[CoBr_4]^{2-}$ are disordered in two positions with occupancy factors 0.754(5) and 0.246(5) (Figure S2).

Table S1. Crystal data for *dppm* and **1**.

	<i>dppm</i>	1
Empirical formula	C ₂₅ H ₂₂ P ₂	C ₇₅ H ₆₆ Br ₄ Co ₂ O ₆ P ₆
Formula weight /g mol ⁻¹	384.36	1686.59
Temperature /K	100(2)	100(2)
Crystal system	orthorhombic	monoclinic
Space group	Pbca	P 1 21/c 1
Crystal size /mm	0.47 x 0.08 x 0.05	0.45 x 0.25 x 0.21
Z	8	4
<i>a</i> / Å	9.7475(3)	13.3702(4)
<i>b</i> / Å	10.2186(4)	19.4278(6)
<i>c</i> / Å	40.1933(11)	28.5245(9)
α / deg	90	90
β / deg	90	90.932(3)
γ / deg	90	90
<i>V</i> /Å ³	4003.5(2)	7408.4(4)
Calculated density <i>D</i> _c /g cm ⁻³	1.275	1.512
Absorption coefficient /mm ⁻¹	2.003	7.661
Reflections collected	26661	75611
Independent reflections	3861	14108
	[R _{int} = 0.0417, R _σ = 0.0385]	[R _{int} = 0.0929, R _σ = 0.1039]
Data/restraints/parameters	3861/0/244	14108/0/854
Goodness-of-fit on F ²	0.905	0.953
Final R indices [I ≥ 2σ (I)]	R ₁ = 0.0295, wR ₂ = 0.0720	R ₁ = 0.0445, wR ₂ = 0.0868
R indices [all data]	R ₁ = 0.0295, wR ₂ = 0.0720	R ₁ = 0.0750, wR ₂ = 0.0900
Largest diff. peak/hole / e Å ⁻³	0.70/-0.23	0.64/-1.19
CCDC No	1526140	1526141

Table S2. Bond lengths (Å) within chromophores of **1**

	Co2	Co2A
Co2-Br1	2.410(11)	2.412(4)
Co2-Br2	2.416(10)	2.408(3)
Co2-Br3	2.392(10)	2.423(3)
Co2-Br4	2.434(9)	2.425(3)
	Co1	
Co1-O1	2.081(3)	
Co1-O5 (<i>trans</i>)	2.102(3)	av, 2.091
Co1-O2	2.125(3)	
Co1-O4 (<i>trans</i>)	2.093(3)	av, 2.109
Co1-O3	2.103(3)	
Co1-O6 (<i>trans</i>)	2.102(3)	av, 2.102

Table S3. Bond angles (deg) in 1.

Br1-Co2-Br2	105.6(5)
Br1-Co2-Br3	108.3(5)
Br1-Co2-Br4	108.8(5)
Br2-Co2-Br3	110.7(4)
Br2-Co2-Br4	110.3(5)
Br3-Co2-Br4	112.9(4)
O1-Co1-O2	92.51(11)
O1-Co1-O3	89.99(11)
O1-Co1-O4	87.22(12)
O1-Co1-O5	177.69(12)
O1-Co1-O6	89.72(11)
O2-Co1-O3	85.80(11)
O2-Co1-O4	177.69(11)
O2-Co1-O5	89.42(11)
O2-Co1-O6	91.82(11)
O3-Co1-O4	91.90(12)
O3-Co1-O5	88.87(11)
O3-Co1-O6	177.59(13)
O4-Co1-O5	90.81(12)
O4-Co1-O6	90.47(12)
O5-Co1-O6	91.50(11)

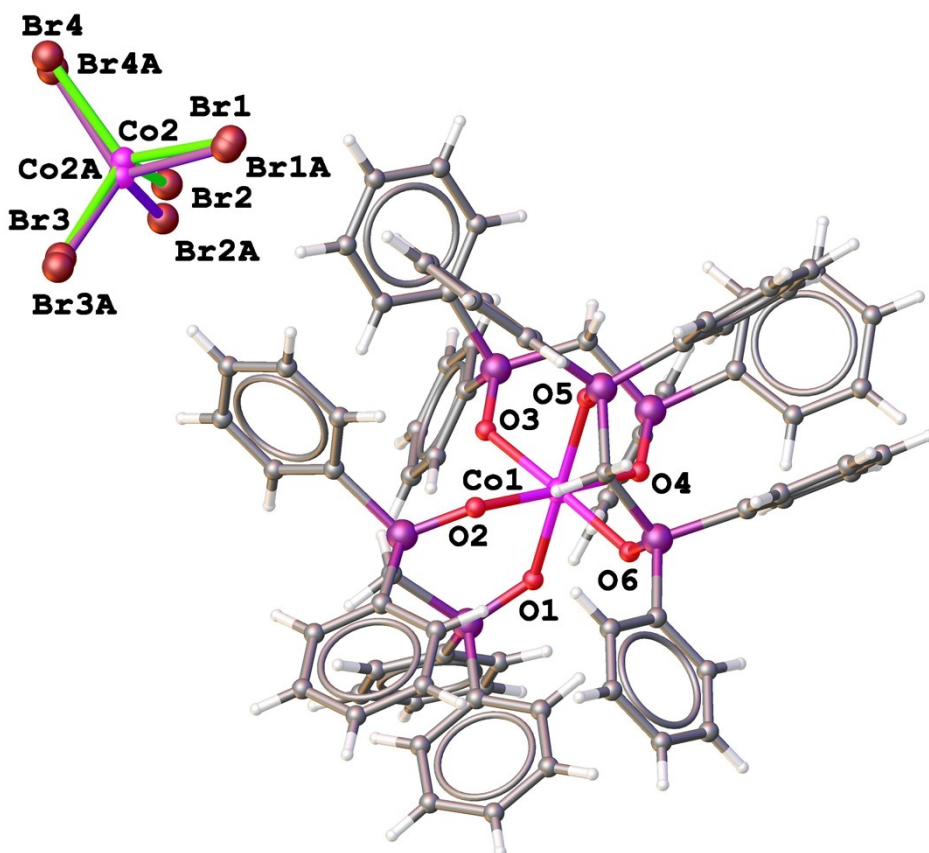


Figure S2. Molecular structure of 1 with labelling atoms of octahedron CoO_6 and tetrahedron $CoBr_4$. The two parts of disordered $[CoBr_4]^{2-}$ anions are labelled using green and violet colour of bonds.

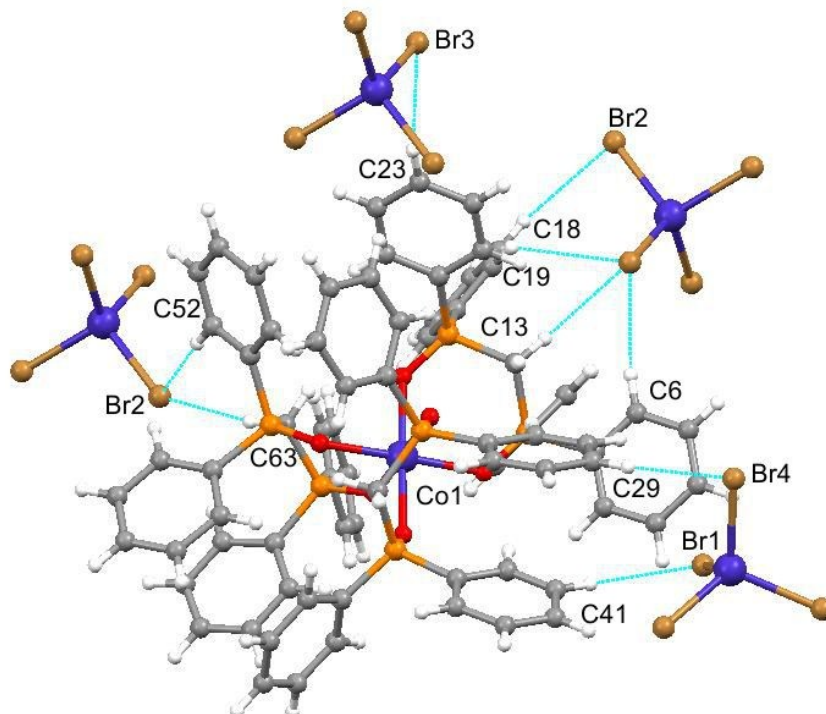


Figure S3. C–H \cdots Br hydrogen bonds (Table S4) in the crystal structure of **1**.

Table S4 Hydrogen Bonds in **1**.

D	H	A	d(D-H)/ \AA	d(H-A)/ \AA	d(D-A)/ \AA	D-H-A/ $^\circ$
C6	H6	Br3 ¹	0.95	2.87	3.804(6)	170
C13	H13A	Br3 ¹	0.99	2.81	3.786(6)	169
C18	H18	Br2 ¹	0.95	2.92	3.826(5)	160
C23	H23	Br3	0.95	2.87	3.792(6)	164
C29	H29	Br4 ²	0.95	3.01	3.950(5)	172
C42	H42	Br3 ²	0.95	3.09	3.902(6)	145
C52	H52	Br2 ³	0.95	2.99	3.939(5)	175
C53	H53	Br4 ³	0.95	3.14	3.975(5)	148
C63	H63A	Br2 ³	0.99	2.69	3.675(4)	171
C69	H69	Br2 ³	0.95	3.10	3.950(5)	150

¹-X,1-Y,1-Z; ²+X,3/2-Y,-1/2+Z; ³1+X,+Y,+Z

[S1] L. Palatinus, G. Chapuis, *J. Appl. Cryst.* **2007**, *40*, 786-790.

[S2] G.M. Sheldrick, *Acta Cryst.* **2015**, *A71*, 3-8.

[S3] G.M. Sheldrick, *Acta Cryst.* **2015**, *C71*, 3-8.

[S4] O.V. Dolomanov, L.J. Bourhis, R.J. Gildea, J.A.K. Howard, H. Puschmann, *J. Appl. Cryst.* **2009**, *42*, 339-341

[S5] C.F. Macrae, I.J. Bruno, J.A. Chisholm, P.R. Edgington, P. McCabe, E. Pidcock, L. Rodriguez-Monge, R. Taylor, J. van de Streek, P.A. Wood, *J. Appl. Cryst.* **2008**, *41*, 466-470.

Spectral data

The FT-IR spectra were measured on ATR holder with highly effective diamond crystal in the region of 4000 - 400 cm^{-1} (Nicolet 5700, Thermo Electron) with DTGS/KBr detector. Far-IR spectra in polyethylene pellets were recorded in the region 50 - 600 cm^{-1} (Nicolet apparatus).

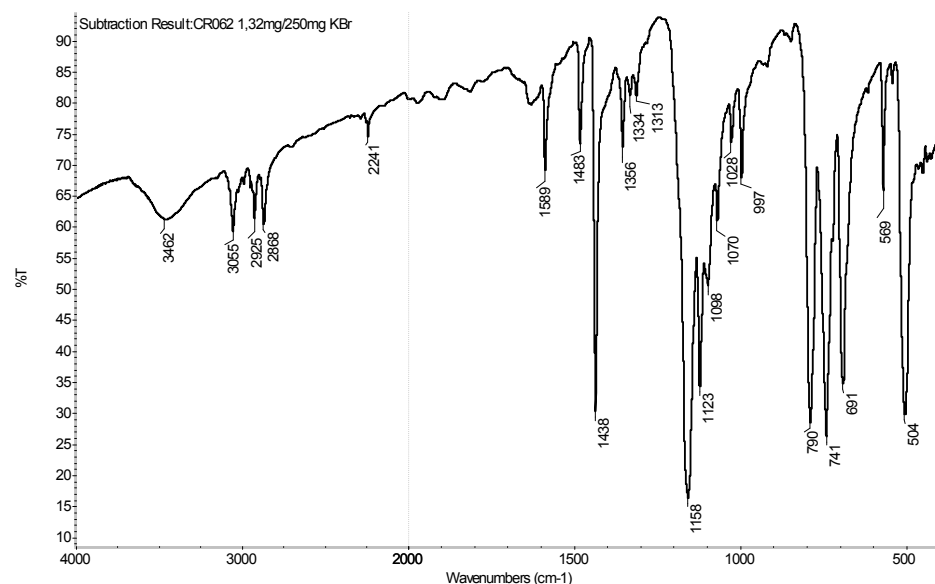


Figure S4. FT-IR spectrum of **1** (400 – 4000 cm^{-1}).

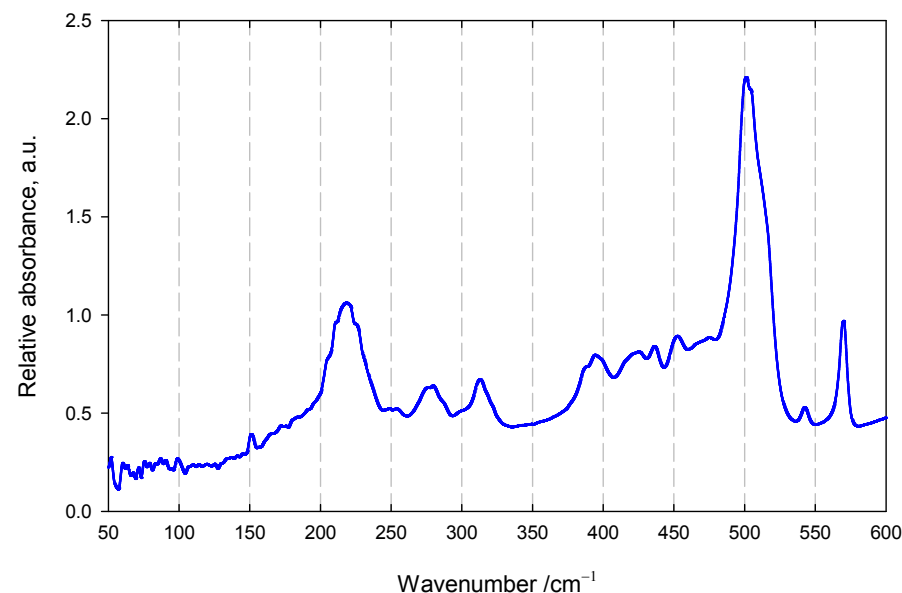


Figure S5. FT-IR spectrum of **1** (50 – 600 cm^{-1}). Three lowest electronic transitions are at 218, 280, 313 cm^{-1} .

Ab initio calculations for the hexacoordinate complex: SOC corrected energies are at 0, 258, 474, 935, 992, and 1130 cm^{-1} . *A posteriori* applied spin Hamiltonian formalism offers $D_0/hc = 129 \text{ cm}^{-1}$ ($E/D = 0.02$) and then $\Delta_0 \sim 260 \text{ cm}^{-1}$.

Magnetic data analysis: $D_0/hc = 147 \text{ cm}^{-1}$, $D_T/hc = 12.3 \text{ cm}^{-1}$; then $\Delta_0 \sim 300 \text{ cm}^{-1}$, $\Delta_T = 25 \text{ cm}^{-1}$.

Magnetometric data on the powder sample down to 2.0 K do not allow a reliable fixation of the E -parameter.

UV-Vis spectra for solid samples dispersed in the Nujol oil were measured by Specord 250 Plus (Analytica Jena) with the DAD detector.

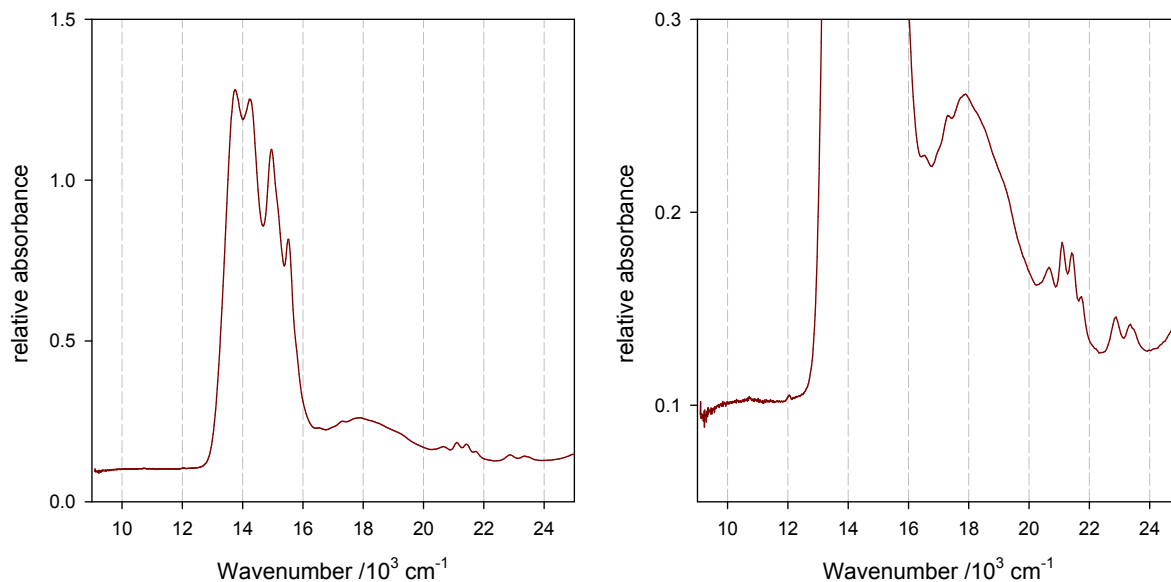


Figure S6. UV-Vis spectrum of **1**. This is a superposition of the $\{\text{CoO}_6\}$ and $\{\text{CoBr}_4\}$ patterns.

- Intense central four-finger pattern between $13\ 000 - 16\ 000 \text{ cm}^{-1}$ refers to the third transition in $[\text{CoBr}_4]^{2-} E_3(^4\text{A}_2 \rightarrow ^4\text{T}_1(\text{P})) \sim 15B + 12Dq(\text{T}_d)$.^{S6} Much weaker, four-finger feature around $21\ 000 \text{ cm}^{-1}$ is due to the spin forbidden doublet transitions.
- Weak feature at $10\ 000 \text{ cm}^{-1}$ is the first transition in nearly octahedral $\{\text{CoO}_6\}$: $E_1(^4\text{T}_{1g} \rightarrow ^4\text{T}_{2g}) \sim 10 Dq(\text{O}_h)$. The second transition at $18\ 000 \text{ cm}^{-1}$ corresponds to $E_2(^4\text{T}_{1g} \rightarrow ^4\text{A}_{2g}) \sim 18 Dq(\text{O}_h)$.
- Additional splitting is due to the lowered symmetry along with the spin-orbit interaction.

[S6] F. A. Cotton, D. M. L. Goodgame and M. Goodgame, *J. Am. Chem. Soc.*, 1961, **83**, 4690.

Ab initio calculations

Table S6. Calculated spin Hamiltonian parameters for three units of **1**.

	Co1 ^a	Co2A ^a	Co2B ^a
$\Delta E_1 / \text{cm}^{-1}$	307	3136	2724
$\Delta E^{\text{SOC}} / \text{cm}^{-1}$	0, 258, 474, 935, 992, 1130	0, 5.2	0, 14.6
g	1.880, 2.569, 2.677	2.346, 2.351, 2.377	2.318, 2.376, 2.421
D / cm^{-1}	129	-2.53	6.57
E/D	0.02	0.11	0.28

^a Three units of **1**; Co1 – hexacoordinate complex; Co2A, Co2B – two disorders of the tetracoordinate anion.

ΔE_1 – first NEVPT2 transition energy. ΔE^{SOC} – SOC corrected transition energies.

Table S7. Calculated NEVPT2 transition energies for unit Co1.

STATE	ROOT	MULT	$\Delta E / \text{cm}^{-1}$
1:	1	4	306.5
2:	2	4	352.0
3:	3	4	6850.5
4:	4	4	7096.1
5:	5	4	7170.2
6:	0	2	12811.0
7:	1	2	13206.2
8:	6	4	14835.5
9:	2	2	18962.3
10:	3	2	19150.6
11:	4	2	19236.8
12:	5	2	19281.4
13:	6	2	19461.5
14:	7	2	19524.8
15:	7	4	20385.7
16:	8	4	20735.4
17:	9	4	21174.8

Table S8. Calculated contributions to spin Hamiltonian parameters for unit Co1.

Block	Mult	Root	D / cm^{-1}	E / cm^{-1}
0	4	0	-0.000	0.000
0	4	1	52.845	40.111
0	4	2	50.350	-35.950
0	4	3	-12.755	-0.702
0	4	4	1.869	0.802
0	4	5	-1.994	2.065
0	4	6	0.001	0.000
0	4	7	0.009	0.003
0	4	8	0.052	-0.051
0	4	9	0.045	0.042
1	2	0	-2.132	2.505
1	2	1	-1.361	-1.320
1	2	2	-0.066	-0.049
1	2	3	-0.293	0.091
1	2	4	-1.134	-0.969
1	2	5	-0.808	0.643
1	2	6	0.005	-0.019
1	2	7	-0.326	0.296

Table S9. Calculated NEVPT2 transition energies for unit Co2A.

STATE	ROOT	MULT	DE/cm ⁻¹
1:	1	4	3135.8
2:	2	4	3151.6
3:	3	4	3275.1
4:	4	4	5150.0
5:	5	4	5541.8
6:	6	4	5747.3
7:	7	4	17867.5
8:	8	4	18089.2
9:	9	4	18158.5
10:	0	2	18721.2
11:	1	2	18753.9
12:	2	2	19038.5
13:	3	2	19092.4
14:	4	2	19105.7
15:	5	2	19750.3
16:	6	2	20940.3
17:	7	2	21019.1

Table S10. Calculated contributions to spin Hamiltonian parameters for unit Co2A.

Block	Mult	Root	D/cm ⁻¹	E/cm ⁻¹
0	4	0	-0.000	0.000
0	4	1	16.420	13.382
0	4	2	-27.947	-1.681
0	4	3	8.823	-12.030
0	4	4	-0.033	-0.007
0	4	5	-0.009	-0.002
0	4	6	0.013	0.012
0	4	7	0.000	0.000
0	4	8	-0.000	0.000
0	4	9	-0.000	-0.000
1	2	0	0.002	0.003
1	2	1	-0.001	0.001
1	2	2	-0.008	-0.003
1	2	3	0.008	-0.000
1	2	4	-0.001	-0.001
1	2	5	-0.001	0.001
1	2	6	-2.706	-2.556
1	2	7	3.250	0.630

Table S11. Calculated NEVPT2 transition energies for unit Co2B.

STATE	ROOT	MULT	DE/cm ⁻¹
1:	1	4	2723.9
2:	2	4	3010.0
3:	3	4	3494.1
4:	4	4	5063.2
5:	5	4	5622.5
6:	6	4	5689.1
7:	7	4	17791.6
8:	8	4	17978.5
9:	9	4	18324.6
10:	0	2	18662.9
11:	1	2	18870.8
12:	2	2	18973.8
13:	3	2	19037.0
14:	4	2	19111.5
15:	5	2	19654.3
16:	6	2	20841.2
17:	7	2	20971.6
18:	8	2	21191.5

Table S12. Calculated contributions to spin Hamiltonian parameters for unit Co2B.

Block	Mult	Root	D/cm ⁻¹	E/cm ⁻¹
0	4	0	-0.000	0.000
0	4	1	19.732	19.502
0	4	2	16.406	-16.913
0	4	3	-29.006	-0.653
0	4	4	0.006	-0.006
0	4	5	-0.017	-0.003
0	4	6	-0.013	-0.001
0	4	7	-0.000	0.000
0	4	8	-0.000	-0.000
0	4	9	0.000	-0.000
1	2	0	-0.005	-0.004
1	2	1	-0.015	0.009
1	2	2	-0.042	0.040
1	2	3	-0.024	-0.011
1	2	4	0.007	-0.001
1	2	5	-0.003	-0.002
1	2	6	-2.583	-2.593
1	2	7	-1.791	2.251
1	2	8	4.177	0.227

Magnetic experiments

- All magnetic measurements were performed using a SQUID magnetometer (Quantum Design, MPMS-XL7).
- The DC susceptibility data was taken at $B_{DC} = 0.1$ in the RSO mode of detection; they were corrected for the underlying diamagnetism and transformed to the effective magnetic moment μ_{eff} .
- The magnetization data was taken until $B = 7$ T at $T = 2.0$ and 4.6 K, respectively; they are presented in the form of the magnetization per formula unit and bohr magneton: $M_1 = M_{mol}/N_A\mu_B$.
- The AC susceptibility data was taken at the oscillating magnetic field $B_{AC} = 0.38$ mT under the applied B_{DC} as indicated throughout for 22 frequencies between $f = 0.1$ and 1500 Hz. Ten scan were averaged and the data spanning outside the 1σ interval was ignored and the rest again averaged and analyzed.

AC magnetic data

Fitting of the AC susceptibility data is based upon 44 data points (22 in-phase and 22 out-of phase) using the formula for the two-set Debye model

$$\chi(\omega) = \chi_S + \frac{\chi_{T1} - \chi_S}{1 + (i\omega\tau_1)^{1-\alpha_1}} + \frac{\chi_{T2} - \chi_{T1}}{1 + (i\omega\tau_2)^{1-\alpha_2}} \quad \text{or} \quad \chi(\omega) = \chi_S + (\chi_T - \chi_S) \left[\frac{x_1}{1 + (i\omega\tau_1)^{1-\alpha_1}} + \frac{1-x_1}{1 + (i\omega\tau_2)^{1-\alpha_2}} \right]$$

where x_1 is the weight of the first, low-frequency relaxation set (channel, branch). This equation decomposes into two explicit formulae for

a) the in phase component

$$\chi'(\omega) = \chi_S + (\chi_{T1} - \chi_S) \frac{1 + (\omega\tau_1)^{1-\alpha_1} \sin(\pi\alpha_1/2)}{1 + 2(\omega\tau_1)^{1-\alpha_1} \sin(\pi\alpha_1/2) + (\omega\tau_1)^{2-2\alpha_1}} + (\chi_{T2} - \chi_{T1}) \frac{1 + (\omega\tau_2)^{1-\alpha_2} \sin(\pi\alpha_2/2)}{1 + 2(\omega\tau_2)^{1-\alpha_2} \sin(\pi\alpha_2/2) + (\omega\tau_2)^{2-2\alpha_2}}$$

b) the out of phase component

$$\chi''(\omega) = (\chi_{T1} - \chi_S) \frac{(\omega\tau_1)^{1-\alpha_1} \cos(\pi\alpha_1/2)}{1 + 2(\omega\tau_1)^{1-\alpha_1} \sin(\pi\alpha_1/2) + (\omega\tau_1)^{2-2\alpha_1}} + (\chi_{T2} - \chi_{T1}) \frac{(\omega\tau_2)^{1-\alpha_2} \cos(\pi\alpha_2/2)}{1 + 2(\omega\tau_2)^{1-\alpha_2} \sin(\pi\alpha_2/2) + (\omega\tau_2)^{2-2\alpha_2}}$$

with the constraint for the isothermal susceptibilities $\chi_{T1} < \chi_{T2}$ in order to get positive contributions from each primitive component. There is $(\chi_{T1} - \chi_S) = (\chi_T - \chi_S)x_1$ and $(\chi_{T2} - \chi_{T1}) = (\chi_T - \chi_S)(1-x_1)$ so that $\chi_{T2} = \chi_T$ and $x_1 = (\chi_{T1} - \chi_S)/(\chi_{T2} - \chi_S) = (\chi_S - \chi_{T1})/(\chi_S - \chi_{T2})$ hold true.

Seven free parameters can be retrieved reliably by using 44 experimental data points.

The functional to be minimized accounts to the relative errors of both susceptibility components

- $F = w \cdot E(\chi') + (1-w) \cdot E(\chi'')$ with the typical weight $w = 0.07$, or
- $F = E(\chi') \cdot E(\chi'')$ with

$$E(\chi) = (1/N) \left[\sum_i^N |(\chi_i^e - \chi_i^c)/\chi_i^e| \right]$$

The optimization routine refers to the genetic algorithm of D. L. Carroll, Univ. Illinois, Urbana, USA, 1998.

The quality of the fit is expressed by

- a) discrepancy factors for the in-phase and out-of phase susceptibilities $R(\chi')$ and $R(\chi'')$ defined as

$$R(\chi) = \sqrt{\left[\sum_i (\chi_i^e - \chi_i^c)^2 \right] / \left[\sum_i (\chi_i^e)^2 \right]}$$

- b) by the standard deviation for each optimized parameter; this is given in parentheses, e.g. 12.3(45) means 12.3 \pm 4.5 (at 95% probability level).

The retrieved parameters should follow a systematic trend along a smooth dependence.

F. Varga, C. Rajnák, J. Titiš, J. Monclo and R. Boča

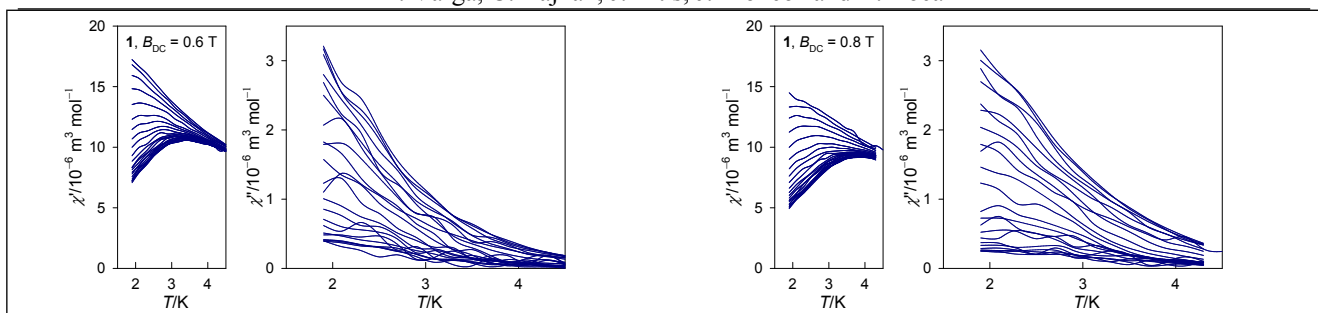


Figure S7. Temperature dependence of the AC susceptibility components for **1**.

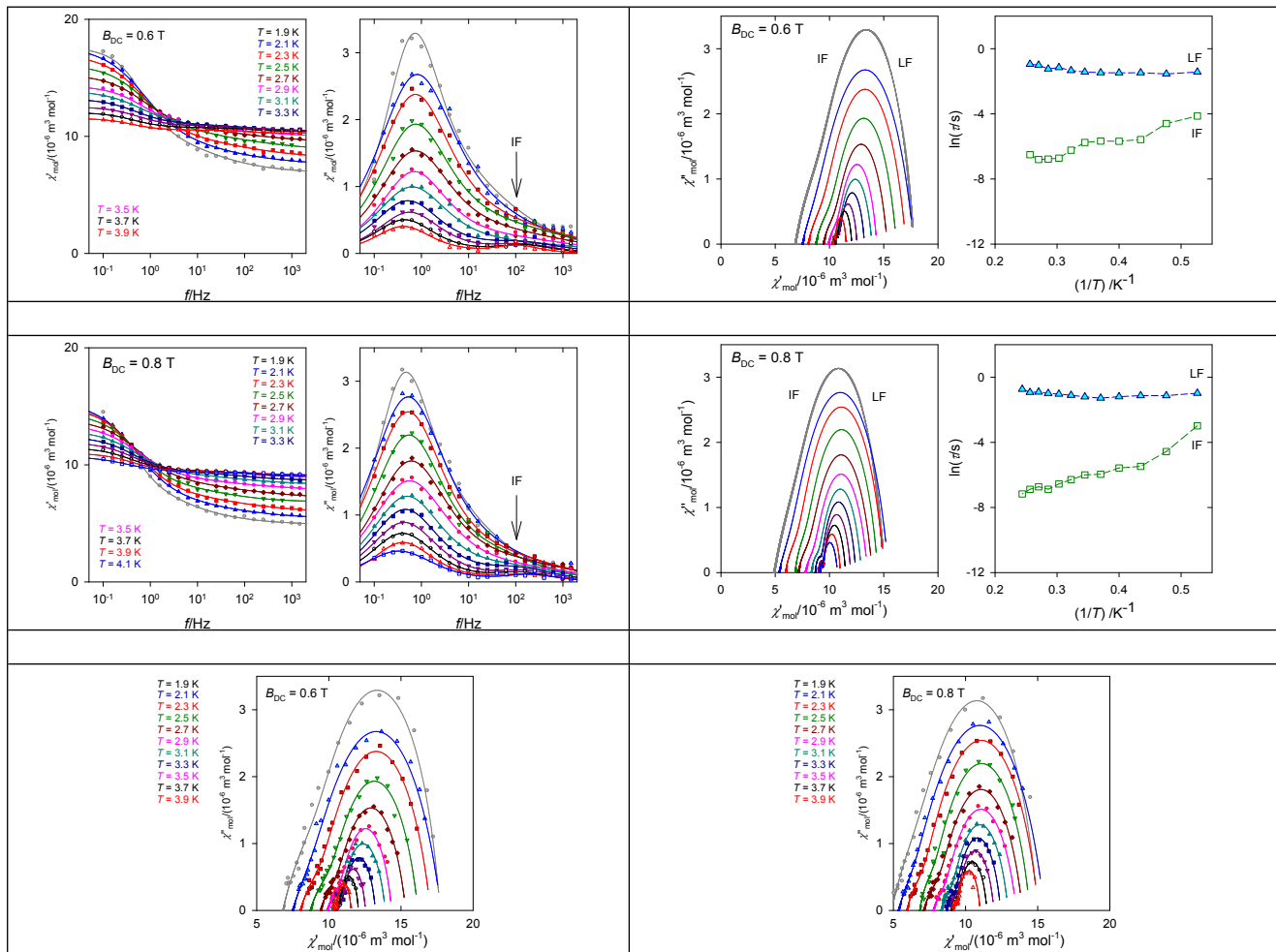


Figure S7. AC susceptibility components for **1** in dependence of the AC frequency. Solid lines – fitted. Symbols – experimental data.

Note. The out-of phase susceptibility component displays a principal low-frequency (LF) peak below $f = 1$ Hz and two satellites: intermediate-frequency (IF) at ca $f = 100$ Hz and an on-set of the high-frequency (HF) at $f > 1500$ Hz. The IF satellite is of a low height (low excess of the isothermal susceptibility χ_{IF}) but it influences the arm of the principal LF peak. Nothing is known about the height of the HF peak as this lies above the hardware limits; consequently the adiabatic susceptibility χ_s in the HF limit cannot be fixed. The fitting procedure was applied with the two-set Debye model considering the LF and IF set for $B_{DC} = 0.6$ and 0.8 T.

Table S13. Parameters of the AC susceptibility for **1** at $B_{DC} = 0.6$ T; fit to LF and IF.

T/K	$R(\chi')$ /%	$R(\chi'')$ /%	χ_S	χ_{LF}	α_{LF}	τ_{LF} $/10^{-3} \text{ s}$	χ_{IF}	α_{IF}	τ_{IF} $/10^{-3} \text{ s}$	x_{LF}
1.9	1.6	6.8	6.8(2)	13.6(35)	0.13(11)	238(21)	17.7(5)	0.51(17)	16(41)	0.62
2.1	1.1	5.3	7.5(4)	15.0(62)	0.28(13)	211(20)	17.8(9)	0.60(34)	10(80)	0.73
2.3	0.78	4.8	8.0(4)	14.6(22)	0.26(6)	228(15)	17.1(3)	0.60(25)	3.8(111)	0.73
2.5	0.74	4.8	8.7(5)	13.9(21)	0.25(7)	226(17)	16.2(3)	0.60(28)	3.4(98)	0.69
2.7	0.70	4.0	9.4(3)	13.6(16)	0.25(7)	228(18)	15.3(2)	0.60(27)	3.4(102)	0.71
2.9	0.84	5.7	9.9(4)	13.1(16)	0.22(9)	239(22)	14.4(2)	0.60(37)	3.2(115)	0.71
3.1	0.50	7.1	10.2(3)	13.1(10)	0.25(7)	262(22)	13.9(1)	0.60(37)	1.9(55)	0.78
3.3	0.43	9.3	10.5(1)	12.7(2)	0.23(3)	313(21)	13.2(7)	0.34(15)	1.2(5)	0.81
3.5	0.47	8.3	10.5(1)	12.2(1)	0.19(3)	287(20)	12.5(6)	0.22(16)	1.1(3)	0.85
3.7	0.44	12	10.4(1)	11.7(1)	0.17(4)	364(29)	12.0(1)	0.15(15)	1.1(3)	0.81
3.9	0.47	12	10.3(1)	11.3(7)	0.14(5)	384(35)	11.5(1)	0.01(15)	1.4(3)	0.83

Table S14. Parameters of the AC susceptibility for **1** at $B_{DC} = 0.8$ T; fit to LF and IF.

T/K	$R(\chi')$ /%	$R(\chi'')$ /%	χ_S	χ_{LF}	α_{LF}	τ_{LF} $/10^{-3} \text{ s}$	χ_{IF}	α_{IF}	τ_{IF} $/10^{-3} \text{ s}$	x_{LF}
1.9	1.8	4.8	4.9(1)	10.8(49)	0.12(16)	376(29)	15.1(8)	0.49(14)	50(166)	0.58
2.1	0.82	2.9	5.3(2)	13.3(23)	0.27(6)	322(16)	15.5(3)	0.59(20)	10(38)	0.78
2.3	1.0	2.9	6.0(2)	13.3(12)	0.26(4)	322(19)	15.1(1)	0.55(18)	4.2(68)	0.80
2.5	3.4	5.4	6.8(4)	13.3(20)	0.26(11)	302(66)	14.5(5)	0.41(55)	3.8(99)	0.84
2.7	0.83	3.3	7.1(3)	12.4(11)	0.27(5)	277(20)	14.0(1)	0.57(22)	2.6(45)	0.77
2.9	0.47	3.5	7.8(2)	12.3(8)	0.29(3)	299(16)	13.5(1)	0.59(20)	2.5(43)	0.79
3.1	0.58	3.1	8.3(1)	12.1(3)	0.26(3)	329(17)	12.9(1)	0.46(14)	1.8(11)	0.83
3.3	0.57	5.9	8.7(1)	11.8(2)	0.24(3)	353(18)	12.4(1)	0.31(13)	1.4(4)	0.84
3.5	0.37	3.6	9.0(1)	11.6(1)	0.23(2)	371(14)	12.0(1)	0.19(9)	1.0(2)	0.87
3.7	0.38	3.4	9.1(1)	11.1(1)	0.21(2)	401(17)	11.5(1)	0.17(10)	1.2(2)	0.83
3.9	0.62	4.6	9.1(1)	10.7(1)	0.17(4)	394(31)	11.0(1)	0.29(20)	1.0(4)	0.84
4.1	0.38	8.7	9.1(1)	10.5(1)	0.25(4)	476(42)	10.7(1)	0.09(13)	0.77(16)	0.88